

Application of Density Functional Theory to line broadening: Cs atoms in liquid helium

Takashi Nakatsukasa*

Physics Department, Tohoku University, Sendai 980-8578, Japan

Kazuhiro Yabana†

*Institute of Physics, University of Tsukuba,
Tennodai 1-1-1, Tsukuba 305-8571, Japan*

George F. Bertsch‡

*Physics Department and Institute for Nuclear Theory,
University of Washington, Seattle, WA 98195, USA*

(Dated: March 6, 2019)

Abstract

We test the applicability of density functional theory (DFT) to spectral perturbations taking an example of a Cs atom surrounded by superfluid helium. The atomic DFT of helium is used to obtain the distribution of helium atoms around the impurity atom, and the electronic DFT is applied to the excitations of the atom, averaging over the ensemble of helium configurations. The shift and broadening of the D_1 and D_2 absorption lines are quite well reproduced by theory, suggesting that the DFT may be useful for describing spectral perturbations in more complex environments.

PACS numbers: 32.70.Jz, 67.40.Yv, 71.15.Mb

*Electronic address: takashi@nucl.phys.tohoku.ac.jp

†Electronic address: yabana@nucl.ph.tsukuba.ac.jp

‡Electronic address: bertsch@phys.washington.edu

I. INTRODUCTION

The time-dependent density-functional theory has proven to be a powerful tool in the description of optical absorption for molecules and clusters in free space (For a review, see Ref. [1]. More recent citations can be found in Refs. [2, 3].). We would like to know whether the theory can be extended to calculate the line shifts and broadening when the absorber is embedded in a medium. Most applications have considered the electronic excitation from a single frozen nuclear configuration representing the ground state of an isolated molecular or an ideal crystal, in which case the predicted absorption lines below the photoionization threshold are sharp. Recently it was shown that the TDDFT also works well in describing the broadening of the transitions and the strength of symmetry-forbidden transitions due to zero-point vibrational motion, taking the example of the benzene spectrum [4]. In the present work, we will calculate the effects of external perturbations on the optical absorption. We choose as a simple test case a Cs atom immersed in liquid helium at low temperature, because of the simplicity both of the electronic structure and of the external perturbation. In the long term we are interested in extending this kind of analysis more complex systems which would require the full power of the time-dependent density functional theory.

Aside from our motivation from the perspective of applications of DFT, spectroscopic measurements of impurity atoms and molecules in superfluid helium have been attracting considerable interest in recent years [5]. The repulsive force between an impurity and helium atoms induces a “bubble” around the impurity. This leads to a weak perturbation of helium atoms on the spectra of impurities. The line shifts and spectral shapes induced by the helium perturbation provide information on the properties of the bubble in the quantum liquid as well as the excited states of the impurity. Since the perturbation is weak, this method also provides a unique opportunity to spectroscopic measurements of atomic clusters at low temperature [6, 7, 8].

The perturbations of Cs lines have been studied experimentally as a function of helium density [9] and we shall calculate this system. There are two *s*-to-*p* transitions, the D_1 ($s_{1/2} \rightarrow p_{1/2}$) and D_2 ($s_{1/2} \rightarrow p_{3/2}$) lines, which are blue-shifted in helium and acquire widths. The shifts and widths of the two lines are different, and the D_2 line has a skewed shape suggesting a double-peak structure. These features were first analyzed with a collective vibration model of the helium bubble [10]. The model reproduced average peak shifts,

but gave line widths less than a half of observed ones. A more sophisticated analysis has been made treating the liquid helium environment by the Path-Integral Monte-Carlo [11]. This quantum simulation has succeeded to reproduce observed D_2 line profiles of the Cs spectra. However, this computation method is very costly in computer resources. We are thus motivated to develop an approach to treat helium perturbation that is both simple and yet has quantitative accuracy. We will show that a density functional theory (DFT) together with a statistical description of helium configurations meets our purpose. The helium density distribution around an embedded atom is calculated with the DFT, and the helium configurations are generated by a random sampling using the density distribution as the sampling weight function.

Besides reporting the calculations on the absorption spectra of Cs in helium, we offer some simple qualitative interpretation of how the qualitative features of the spectrum reflect the properties of the helium bubble around the atom.

II. FORMALISM

A. Description of liquid helium around an impurity atom

Among number of density functional methods for liquid helium, we adopt the Orsay-Paris functional of Ref. [12]. Although the Orsay-Paris functional is known to have some problems with dynamic properties of liquid helium [13], it has a correct long-range behavior and reasonable short-range characteristics. Since we are interested in a density profile of liquid helium, it should be adequate for our purposes.

The energy in the DFT is assumed to have the form

$$E = \int d\mathbf{r} \mathcal{H}_0(\mathbf{r}), \quad (1)$$

where

$$\mathcal{H}_0(\mathbf{r}) = \frac{1}{2m} \left| \nabla \sqrt{\rho(\mathbf{r})} \right|^2 + \frac{1}{2} \int d\mathbf{r}' \rho(\mathbf{r}) \rho(\mathbf{r}') V_{\text{LJ}}(|\mathbf{r} - \mathbf{r}'|) + \frac{c}{2} \rho(\mathbf{r}) (\bar{\rho}_{\mathbf{r}})^{1+\gamma}. \quad (2)$$

Here, m is the mass of a helium atom and $\bar{\rho}_{\mathbf{r}}$ is a coarse-grained density defined by

$$\bar{\rho}_{\mathbf{r}} = \frac{3}{4\pi h^3} \int_{r < h} d\mathbf{r} \rho(\mathbf{r}). \quad (3)$$

The V_{LJ} is a standard Lennard-Jones potential describing the He-He interaction screened at distances shorter than the distance h ,

$$V_{\text{LJ}}(|\mathbf{r} - \mathbf{r}'|) = \begin{cases} 4\epsilon \left[\left(\frac{\alpha}{|\mathbf{r} - \mathbf{r}'|} \right)^{12} - \left(\frac{\alpha}{|\mathbf{r} - \mathbf{r}'|} \right)^6 \right], & \text{for } |\mathbf{r} - \mathbf{r}'| \geq h, \\ V_{\text{LJ}}(h) \left(\frac{|\mathbf{r} - \mathbf{r}'|}{h} \right)^4, & \text{for } |\mathbf{r} - \mathbf{r}'| < h. \end{cases} \quad (4)$$

The values of the parameters in Eqs. (2), (3), and (4) are $c = 1.04554 \times 10^7 \text{ K}\text{\AA}^{3(1+\gamma)}$, $\gamma = 2.8$, $\epsilon = 10.22 \text{ K}$, $\alpha = 2.556 \text{ \AA}$, and $h = 2.377 \text{ \AA}$. This is the same density functional that was used in Ref. [14] to study atomic impurities in liquid helium. In that work, the effect of the impurity was treated by including a potential interaction $V_I(r)$ between it and the helium atoms in the density functional,

$$\mathcal{H}(\mathbf{r}) = \mathcal{H}_0(\mathbf{r}) + V_I(\mathbf{r})\rho(\mathbf{r}), \quad (5)$$

The $V_I(r)$ has important contributions from the repulsive between electrons and the helium atoms, as well as the Van der Waals-type polarization interaction. Since we need to treat interaction of impurity electrons with the helium atoms explicitly later on when we calculate the electronic excitation, we introduce it here as well for calculating the helium distribution. We approximate it as a contact interaction, i.e. of the form

$$V_{\text{e-He}}(\mathbf{r}_e - \mathbf{r}) = V_0\delta(\mathbf{r}_e - \mathbf{r}), \quad (6)$$

where \mathbf{r}_e and \mathbf{r} are coordinates of the electron and helium atom, respectively. The strength V_0 is determined from the electron-helium scattering length a as

$$V_0 = \frac{2\pi a}{m_e}, \quad (7)$$

where m_e is the electron mass. Then $V_I(\mathbf{r})$ is given by

$$V_I(\mathbf{r}) = V_0\rho_e(\mathbf{r}). \quad (8)$$

where $\rho_e(\mathbf{r})$ is the electron density of the impurity atom. We take $a = 0.69 \text{ \AA}$, corresponding the observed low-energy electron-helium cross section $\sigma = 6.0 \text{ \AA}^2$ [15]. We have also assumed that the ion core is heavy enough to be treated as a classical particle at the origin. Since Eq. (6) expresses the interaction between He atoms and an electron, the same interaction will be used to estimate the energy shift of valence electrons due to the helium perturbation.

This treatment of interatomic potential ignores long-range attraction due to the polarization effects. The influence of the polarization effect will be mentioned later.

Utilizing the energy functional, $E[\rho] = \int d\mathbf{r} \mathcal{H}(\mathbf{r})$, we calculate the density profile of liquid helium, putting the impurity atom at the origin. Minimizing the grand potential at zero temperature, $\Omega \equiv E[\rho(\mathbf{r})] - \mu N$, leads to a Hartree-type equation

$$\left[-\frac{1}{2m} \nabla^2 + U(\mathbf{r}) + V_I(\mathbf{r}) \right] \sqrt{\rho(\mathbf{r})} = \mu \sqrt{\rho(\mathbf{r})}, \quad (9)$$

where

$$U(\mathbf{r}) \equiv \int d\mathbf{r}' \rho(\mathbf{r}') V_{\text{LJ}}(|\mathbf{r} - \mathbf{r}'|) + \frac{c}{2} (\bar{\rho}_{\mathbf{r}})^{\gamma+1} + \frac{c}{2} (1 + \gamma) \frac{3}{4\pi h^3} \int_{|\mathbf{r}-\mathbf{r}'|<h} d\mathbf{r}' \rho(\mathbf{r}') (\bar{\rho}_{\mathbf{r}})^{\gamma}. \quad (10)$$

The equation is solved with the boundary condition that the density go to the bulk density ρ_0 at large \mathbf{r} , which can be satisfied setting the chemical potential to

$$\mu = b\rho_0 + \left(1 + \frac{\gamma}{2}\right) c\rho_0^{\gamma+1}, \quad (11)$$

where $b = \int d\mathbf{r} V_{\text{LJ}}(\mathbf{r}) = -8.8881 \times 10^2 \text{ K}\text{\AA}^3$. The bulk density is related to the pressure P by

$$P = -\frac{\partial E}{\partial V} = \frac{1}{2} b \rho_0^2 + \frac{\gamma+1}{2} c \rho_0^{\gamma+2}. \quad (12)$$

Carrying out the solution of Eq. (9) we find the density profile shown in Fig. 1. The three curves give $\rho(r)$ at equilibrium densities ρ_0 of 0.0218, 0.0239, and 0.0253 \AA^{-3} , corresponding to $P = 0, 10$, and 20 atm , respectively. One can see a sharp rise in the density at $r \approx 6 \text{ \AA}$. This corresponds to the bubble radius. An oscillatory structure appears on the density profile, especially under high pressure. This feature is different from that of a bubble model adopted in Refs. [9, 10]. The maximum value of the density for $P = 20 \text{ atm}$ is about 0.0275 \AA^{-3} at $r = 7.2 \text{ \AA}$.

We use the $\rho(r)$ computed above to generate configurations of helium atoms as follows. Take a large volume surrounding the alkali atom and denote it as V . This volume includes N helium atoms in average, where N is given by $\int_V d\mathbf{r} \rho(\mathbf{r}) = N$. We randomly sample N helium positions in V according to the density distribution $\rho(\mathbf{r})$. This sampling procedure gives probability distribution without correlation among helium atoms. Denoting $f(\mathbf{r}) = \rho(\mathbf{r})/N$, the probability distribution of N atoms is given by

$$w_{\text{nc}}(\boldsymbol{\tau}) = \prod_{i=1}^N f(\mathbf{r}_i), \quad (13)$$

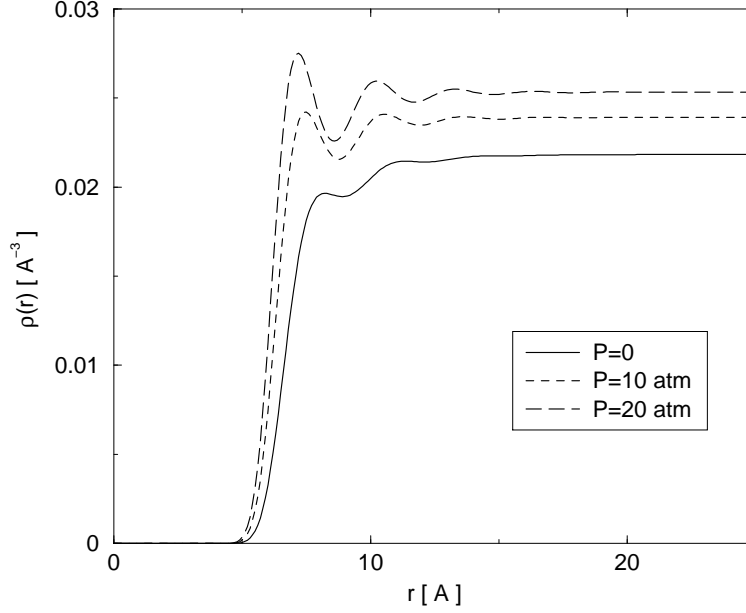


FIG. 1: Helium density profile around Cs atom. The coordinate r represents the distance from the Cs atom.

where $\boldsymbol{\tau}$ stands for $(\mathbf{r}_1, \dots, \mathbf{r}_N)$. We will also study the effect of helium-helium correlations by considering a probability distribution of the form

$$w_c(\boldsymbol{\tau}) = \prod_{i=1}^N g(\mathbf{r}_i) \prod_{i<j}^N \theta(r_{ij} - d). \quad (14)$$

Here d is the range of a short-range correlation. The distribution function $g(\mathbf{r})$ is determined by the condition that the distribution of Eq. (14) gives a helium density $\rho(\mathbf{r})$,

$$\rho(\mathbf{r}) = N \int_V d\mathbf{r}_2 \cdots d\mathbf{r}_N w_c(\mathbf{r}, \mathbf{r}_2, \dots, \mathbf{r}_N). \quad (15)$$

In practice, we employ an iterative procedure to find $g(\mathbf{r})$ from this condition.

B. Helium perturbation on the atomic spectra

In the previous section, we described a density functional theory for calculating the density profile of liquid helium $\rho(\mathbf{r})$, and taking account of the effect of an impurity atom at the origin. In this section, we discuss the calculation of the atomic spectrum, including the effects of the helium atoms.

We begin with the theory of the isolated atom. Orbital wave functions are calculated using density functional theory with Dirac wave functions and kinetic energy operator. We need

accurate wave functions at large distances from the atom, which cannot be achieved with the traditional LDA functional due to the incorrect orbital eigenvalues and the incorrect asymptotic behavior of the potential. As is well known, these problems are diminished with the GGA density functionals. We employ the GGA functional of Ref. [16], which has a gradient correction to produce correct asymptotic behavior of the potential. The gradient correction includes an adjustable parameter β ; we utilize this freedom to make the orbital energy coincide with the measured one. For the $s_{1/2}$ orbital, the orbital energy is set equal to the ionization potential of Cs atom, 3.89 eV. For the $p_{1/2}$ and $p_{3/2}$ orbitals, the orbital energies are set equal to the ionization potential minus the excitation energies (about 1.43 eV). The quality of the wave function may be tested by examining the transition oscillator strength. For D_1 and D_2 transitions, the calculated oscillator strength assuming a pure single-electron transition is 1.034, in good agreement with measured value, 1.058. The calculated electron density distributions are shown in Fig. 2. In principle, there will be contributions to the transition from core electrons as well that can be taken into account with the TDDFT. Applying the TDDFT to the present case, the core contributions reduce the oscillator strength by some tens of percent, but do not significantly affect the asymptotic wave function of the valence electron. We therefore use the simpler single-electron wave functions below rather than wave functions from the TDDFT.

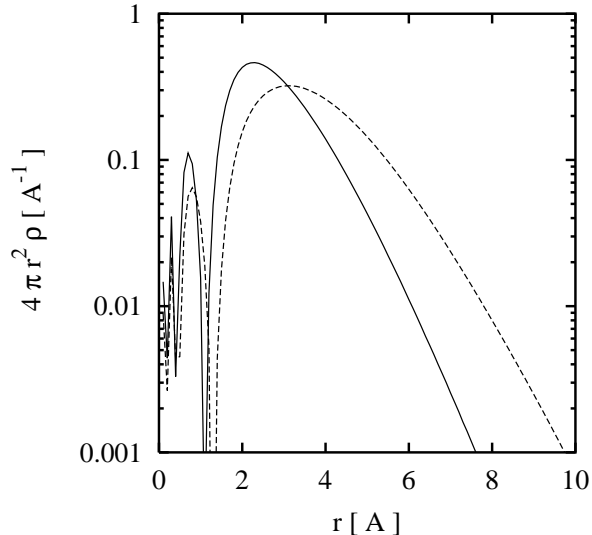


FIG. 2: Electron density distribution of the $s_{1/2}$ (solid) and $p_{1/2}$ orbitals of Cs. See text for details of the calculation.

For a given configuration of helium atoms, $\boldsymbol{\tau} = (\mathbf{r}_1, \dots, \mathbf{r}_N)$, we evaluate shifts of orbital energies with first order perturbation theory. We use the same helium configuration for the ground state $s_{1/2}$ and excited states $p_{1/2}$ and $p_{3/2}$, following the Frank-Condon principle. For $s_{1/2}$ and $p_{1/2}$ states, the energy shifts of the valence electron is calculated as

$$\Delta E^{(k)}(\boldsymbol{\tau}) = \langle \psi^{(k)} | \sum_i V_{e-\text{He}}(i) | \psi^{(k)} \rangle = \sum_i V_0 |\psi^{(k)}(\mathbf{r}_i)|^2 \quad (16)$$

where k stands for orbital quantum numbers (ℓj) and either m state may be taken. For $p_{3/2}$ states, the matrix elements depend on m and we have to diagonalize a 4×4 matrix to get the energy shifts. We then obtain two eigenenergies, each of which is doubly degenerate.

Each helium configuration produces an energy shift and possible splitting but the transitions remain sharp. The line broadening comes from the ensemble average over helium configurations. The line shape of the spectra for D_1 ($s_{1/2} \rightarrow p_{1/2}$) transition is given by

$$S_{D_1}(E) = \int_V d\boldsymbol{\tau} w(\boldsymbol{\tau}) \delta(E - (\Delta E^{(p_{1/2})}(\boldsymbol{\tau}) - \Delta E^{(s_{1/2})}(\boldsymbol{\tau}))), \quad (17)$$

where E is a shift from the energy position of the free atom. For the D_2 ($s_{1/2} \rightarrow p_{3/2}$) transition, we need to add the two eigenmodes,

$$S_{D_2}(E) = \int_V d\boldsymbol{\tau} w(\boldsymbol{\tau}) \left\{ \delta \left(E - \left(\Delta E_1^{(p_{3/2})}(\boldsymbol{\tau}) - \Delta E^{(s_{1/2})}(\boldsymbol{\tau}) \right) \right) + \delta \left(E - \left(\Delta E_2^{(p_{3/2})}(\boldsymbol{\tau}) - \Delta E^{(s_{1/2})}(\boldsymbol{\tau}) \right) \right) \right\}. \quad (18)$$

C. Origin of peak shifts, broadening, and splitting

In this section, we discuss qualitatively argument how the blue shifts, the broadening of the lines, and the splitting of D_2 transitions occur. First consider a valence electron of the alkali atom interacting with a single helium atom at a position \mathbf{R} with respect to the impurity atom. The energy shift of the valence electron is determined by the electron wave function at the position of helium atom, $\psi(\mathbf{r}_e = \mathbf{R})$.

For $s_{1/2}$ and $p_{1/2}$ states, the energy shift $\Delta\epsilon$ is calculated as

$$\Delta\epsilon^{(k)} = V_0 \rho_e^{(k)}(R), \quad (19)$$

as the first-order perturbation by $V_{e-\text{He}}$. Since V_0 is positive, the energy shift, Eq. (19), is also positive. As may be seen from Fig. 2, the wave function of the $p_{1/2}$ state is considerably

larger than the $s_{1/2}$ state outside the bubble. Thus, we expect a blue shift of D_1 excitation spectra, $\Delta\epsilon^{(p_{1/2})} - \Delta\epsilon^{(s_{1/2})} > 0$.

For $p_{3/2}$ states, the situation is slightly more complicated, because, in general, there are off-diagonal matrix elements among degenerate states with different m . However, all the off-diagonal elements vanish if we assume that the helium atom lies on the Z -axis, $X = Y = 0$ and $Z = R$. We lose no generality in the case of a single helium atom. The helium atom at $Z = R$ produces an energy shift $\Delta\epsilon$ as

$$\Delta\epsilon_m^{(p_{3/2})} = \langle \psi_m^{(p_{3/2})} | V_{e-\text{He}} | \psi_m^{(p_{3/2})} \rangle = \begin{cases} 2V_0\bar{\rho}_e^{(p_{3/2})}, & \text{for } |m| = 1/2, \\ 0, & \text{for } |m| = 3/2. \end{cases} \quad (20)$$

where $\bar{\rho}^{(k)}$ is the angle-average electron density. There is no shift for $|m| = 3/2$ states in the first-order perturbation by $V_{e-\text{He}}$. As a result, the D_2 transition splits into two peaks; one has a blue shift, $\Delta\epsilon_{|m|=1/2}^{(p_{3/2})} - \Delta\epsilon^{(s_{1/2})} > 0$, and the other has a small red shift, $-\Delta\epsilon^{(s_{1/2})} < 0$. In fact we can neglect $-\Delta\epsilon^{(s_{1/2})}$ in comparison to the other shifts due to the large distance of the perturbing helium atom. Also one can neglect the small energy difference between the two spin orbit partners. Then the energy shift of $|m| = 1/2$ states is twice of that of $p_{1/2}$ states. Note that the average shift of the D_2 components is the same as the D_1 line. In summary, a helium atom at a distance R shifts the D_1 transition by $\Delta \equiv V_0\bar{\rho}_e^{(p_{1/2})}(R)$. The energy of D_2 transition splits into two: one has no shift and the other is shifted by 2Δ . This explains qualitatively the overall blue shift of both lines and the skewed profile of the D_2 line.

However, while the observed D_2 line shape can be analyzed as a sum of two components, both components are blue shifted roughly the same amount as the D_1 line. This shows the shift is due to the simultaneous interaction with several helium atoms. For example, if two helium atoms are at $(R, 0, 0)$ and at $(0, 0, R)$, again, a D_2 line splits into two. However, in this case, both have blue shifts (Δ and 3Δ). If three helium atoms are at $(R, 0, 0)$, $(0, R, 0)$, and $(0, 0, R)$, then, D_2 line shows a blue shift of 3Δ but no splitting. Roughly speaking, the magnitude of line shift is determined by number of helium atoms contributing to the perturbation and the splitting is determined by anisotropy of the helium configuration which increases as the square root of the number of atoms, assuming that there are no correlations between atoms. The average energy shift remains the same for the D_1 and D_2 lines, irrespective of the number of helium atoms causing the perturbation.

III. NUMERICAL RESULTS

To calculate line shapes of the Cs D transition in a helium, we evaluated Eq. (2.18) and (2.19) by sampling 100 000 helium configurations, generated according to the density profiles in Fig. 1. The calculated energy shifts are added to the observed D lines of free Cs atom ($\lambda = 894.9$ nm for D_1 and 852.7 nm for D_2). Then, the intensity is estimated by counting number of events in bins of wavelength $\Delta\lambda = 0.1$ nm. The obtained intensity spectra are shown in Fig. 3. The D_1 line can be well approximated by a single Gaussian, although there is a slightly larger tail at high-energy (low-wavelength) side. On the other hand, the D_2 line has a double-peaked structure. This feature agrees with the experimental observation [9, 10].

Fig. 4 shows the pressure dependence of the peak shift and broadening of the D_1 excitation lines. The peak shift reproduces the observed pressure dependence, but comes out about 20% lower than measured. The difference could be due to an incorrect asymptotic wave function in the Cs atom; only a 10% error in the wave function would be required to explain the difference. Or the calculated helium bubble might be too large. Here, decreasing the size of the bubble by 0.3 Å out of 6 Å would be sufficient to produce the measured peak shift. We shall return to this later. The line broadening comes out better than would be expected, given the quality of agreement for the peak shift. The agreement here shows that the fluctuations of the helium distribution are well described by the model adopted.

A qualitative measure of the fluctuations can be constructed by defining an effective number of helium atoms that contribute to the perturbation. Calling the shift from an individual helium atom $\Delta(i)$, the total shift is

$$\Delta E = \sum_{i=1}^N \Delta(i) \quad (21)$$

and the effective number M_{eff} is defined as

$$M_{\text{eff}} \equiv \left\langle \frac{(\sum_i \Delta(i))^2}{\sum_i \Delta(i)^2} \right\rangle, \quad (22)$$

where $\langle \dots \rangle$ indicates the ensemble average. The calculation leads to $M_{\text{eff}} \approx 8$ for $s_{1/2}$ state at $P = 0$, increasing to 11-12 at $P = 25$ atm. The M_{eff} can be compared with number of helium atoms in the first shell of density profile (Fig. 1). The average numbers of helium atoms in a region of $r < 8.5$ Å are 27 at $P = 0$ and 45 at $P = 25$ atm. M_{eff} turns out

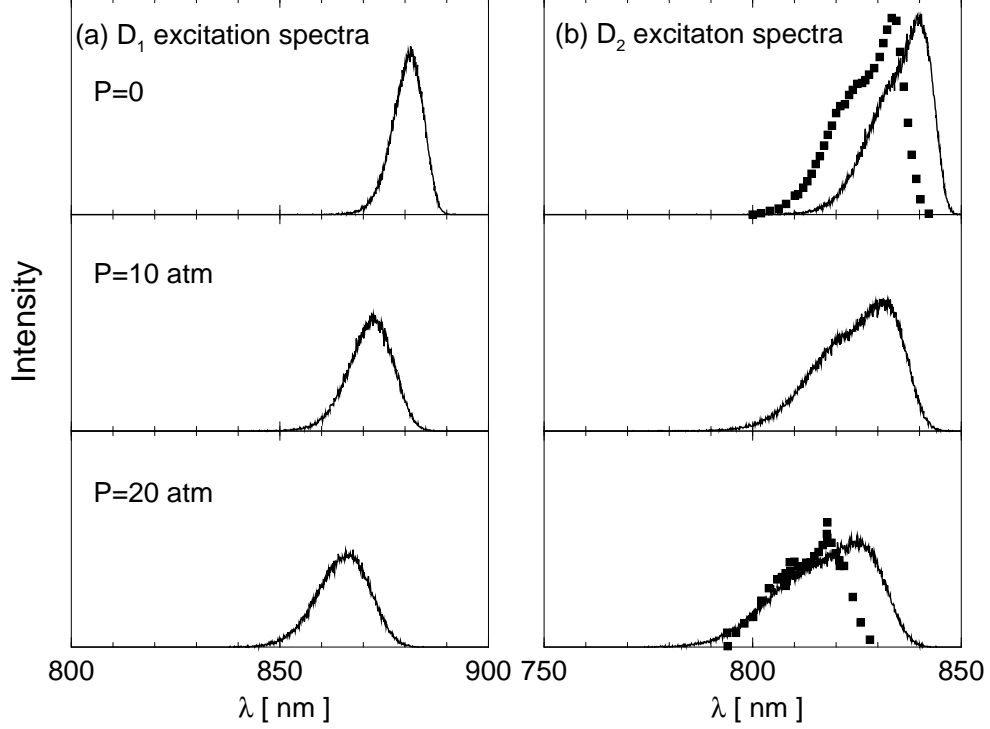


FIG. 3: (a) Cs D_1 excitation spectra at different helium pressure; $P = 0, 10$, and 20 atm (b) The same as (a) but for D_2 excitation spectra. Experimental data from Ref. [9] are plotted as filled squares.

to be much smaller than the number in the first shell. Therefore, we may say that the perturbation on the valence electron is dominated by a small number of helium atoms in the inner surface of a bubble. This fact indicates the importance of treating the perturbation from individual helium atoms in describing fluctuation effect.

We can also understand the order of magnitude of the fluctuation effects using M_{eff} . Assuming independent helium atoms, the fluctuations are proportional to $1/\sqrt{M_{\text{eff}}}$. Thus we would expect that widths of the lines and the splitting of the components of the D_2 would be proportional to the average shift times that quantity. In fact the D_1 width is about $1/2$ of its average shift in the zero pressure data, to be compared with $1/\sqrt{M_{\text{eff}}} \approx 1/3$. Ref. [9] analyzes the D_2 line shape as a sum two Gaussian peaks. For the measurements at low pressure, the splitting of the components relative to the average shift is just $1/3$, agreeing with our very crude argument.

In order to investigate effects of the polarization potential that we so neglected, we consider also a helium-Cs interaction that includes the van der Waals terms [17]. Once the

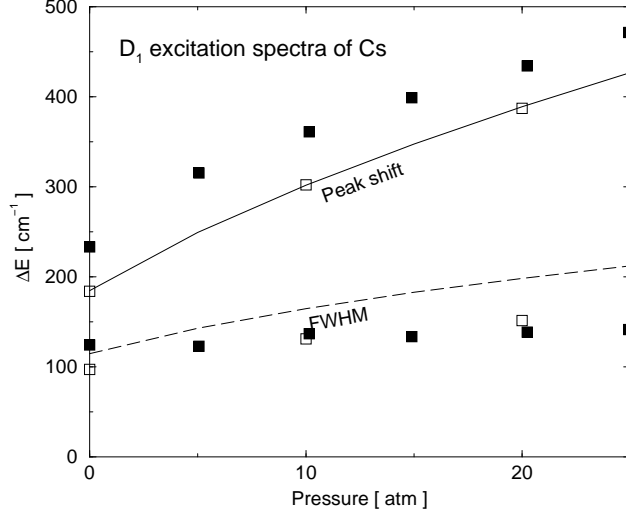


FIG. 4: Pressure shift (solid line) and broadening (dashed line) of the D_1 excitation spectra of Cs as a function of helium pressure. Open squares represent broadening calculated with He-He correlations at $P = 0, 10$, and 20 atm. The experimental data are plotted as filled squares.

density profile $\rho(\mathbf{r})$ is determined, we use the interaction between a valence electron and helium, Eq. (6), to calculate the atomic spectra. We find that potential of Ref. [17] gives a reduced radius for the helium bubble at zero pressure, by about 0.3 \AA . As a result, the blue shift increases by about 35 cm^{-1} at $P = 0$, which fits the experimental data very well. The line width is also slightly increased. This enhancement of blue shifts is decreasing as the pressure is increasing. The calculation shows almost no additional shift at $P=20$ atm.

Next, let us discuss effects of correlations among helium atoms. The He-He correlation should influence the line width because it removes some part of fluctuations of the He configuration. Roughly speaking, the radial fluctuation controls the line width and the angle fluctuation determines the skewness of D_2 line. To test this, we sample the helium configurations using the probability distribution of Eq. (14), taking $d = 2.377 \text{ \AA}$. We construct the distribution function $g(\mathbf{r})$ in Eq. (14), so as to reproduce the density profile $\rho(\mathbf{r})$ determined by the DFT, Eq. (9). The results are displayed in Fig. 5 and also in Fig. 4 with open squares. The correlation effect does not change the average peak positions at all. However, it reduces the line widths, especially when the liquid helium is under high pressure. At $P = 20$ atm, the FWHM of D_1 line is calculated to be 150 cm^{-1} , which well agrees with the experiment (140 cm^{-1}). The skewness of D_2 line also becomes smaller.

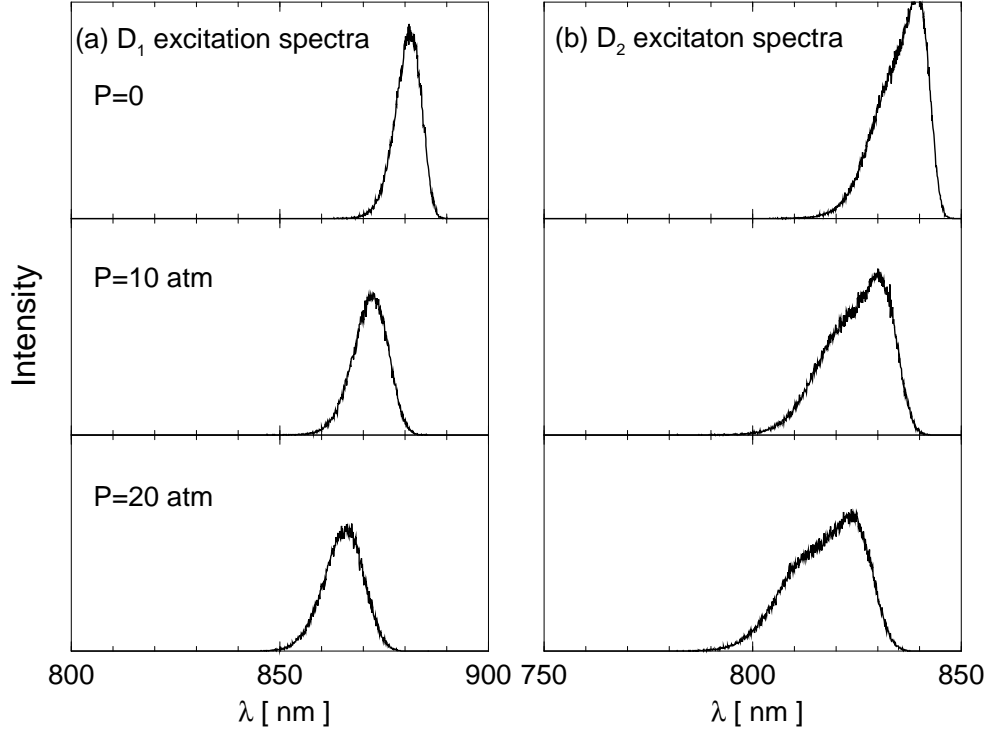


FIG. 5: (a) Cs D_1 excitation spectra and (b) D_2 excitation spectra as in Fig. 2, with inclusion of He-He correlations. See text for explanation.

IV. SUMMARY

We have developed a simple model to describe atomic spectra of impurities embedded in the superfluid helium. Our description employs a density functional theory for the helium distribution, and treats helium configurations statistically. The model is applied to the spectra of Cs atom embedded in superfluid helium. Various features in the spectra, which include line shifts, broadening, and skewness, are nicely reproduced in our calculation without any adjustable parameters. Thus we are confident that our model includes basic physical elements of the helium perturbation correctly. Since the model is simple enough to apply to more complex systems such as molecules and clusters, we wish to analyze these systems in future.

Acknowledgments

One of authors (T.N.) thanks Y. Matsuo, Y. Fukuyama, and R. Sanetou for discussions. K.Y. acknowledges financial support by the Ministry of Education, Culture, Sports, Science and Technology of Japan, Contract No. 11640372. G.F.B. acknowledges conversations with P.G. Reinhard and J. Rehr, and support from the US Department of Energy under Grant DE-FG06-90ER40561.

- [1] M. E. Casida, in *Recent developments and applications of modern density functional theory*, edited by J. Seminario (Elsevier, Amsterdam, 1996), vol. 4, p. 391.
- [2] G. B. K. Yabana, *Int. J. Quant. Chem.* **75**, 55 (1999).
- [3] T. Nakatsukasa and K. Yabana, *J. Chem. Phys.* **114**, 2550 (2001).
- [4] K. Y. G. F. Bertsch, A. Schnell, *J. Chem. Phys.* **115**, 4051 (2001).
- [5] A. F. V. J. P. Toennies, *Annu. Rev. Phys. Chem.* **49**, 1 (1998).
- [6] J. L. Persson, Q. Hui, M. Nakamura, and M. Takami, *Phys. Rev. A* **52**, 2011 (1995).
- [7] J. Higgins, W. Ernst, C. Callegari, J. Reho, K. K. Lehmann, G. Scoles, and M. Gutowski, *Phys. Rev. Lett.* **77**, 4532 (1996).
- [8] A. Bartelt, J. D. Close, F. Federmann, N. Quaas, and J. P. Toennies, *Phys. Rev. Lett.* **77**, 3525 (1996).
- [9] T. Kinoshita, K. Fukuda, Y. Takahashi, and T. Yabuzaki, *Phys. Rev. A* **52**, 2707 (1995).
- [10] T. Y. T. Kinoshita, K. Fukuda, *Phys. Rev. B* **54**, 6600 (1996).
- [11] S. Ogata, *J. Phys. Soc. Jpn.* **68**, 2153 (1999).
- [12] J. Dupont-Roc, M. Himbert, N. Pavloff, and J. Treiner, *J. Low Temp. Phys.* **81**, 31 (1990).
- [13] J. T. L. Pricaupenko, *J. Low Temp. Phys.* **96**, 19 (1994).
- [14] F. Dalfovo, *Z. Phys. D* **29**, 61 (1994).
- [15] I. K. S. Trajmar, J.W. McConkey, in *Atomic, Molecular and Optical Physics Handbook*, edited by G. Drake (AIP Press, NY, 1996), p. 717.
- [16] E. J. B. R. van Leeuwen, *Phys. Rev. A* **49**, 2421 (1994).
- [17] S. H. Patil, *J. Chem. Phys.* **94**, 8089 (1991).